Journal of Molecular Graphics and Modelling 44 (2013) 220–231

Contents lists available at SciVerse ScienceDirect

Journal of Molecular Graphics and Modelling

journal homepage: www.elsevier.com/locate/JMGM

# *In silico* design: Extended molecular dynamic simulations of a new series of dually acting inhibitors against EGFR and HER2

Marawan Ahmed[a,*], Maiada M. Sadek[b], Khaled A. Abouzid[c], Feng Wang[a,**]

[a] *eChemistry Laboratory, Faculty of Life and Social Sciences, Swinburne University of Technology, Hawthorn, Melbourne, Victoria 3122, Australia*
[b] *Pharmaceutical Organic Chemistry, Faculty of Pharmacy, MSA University, 6th October, Egypt*
[c] *Pharmaceutical Chemistry Department, Faculty of Pharmacy, Ain Shams University, Cairo 11566, Egypt*

ARTICLE INFO

*Article history:*
Accepted 17 June 2013
Available online 3 July 2013

*Keywords:*
Tyrosine kinase
EGFR/HER2
Molecular dynamics
Water occupancy
AM1-D

ABSTRACT

Based on the hit structures that have been identified in our previous studies against EGFR and HER2, new potential inhibitors that share the same scaffold of the hit structures are designed and screened *in silico*. Insights into understanding the potential inhibitory effect of the new inhibitors against both EGFR and HER2 receptors is obtained using extended molecular dynamics (MD) simulations and different scoring techniques. The binding mechanisms and dynamics are detailed with respect to two approved inhibitors against EGFR (lapatinib) and HER2 (SYR127063). The best scoring inhibitor (T9) is chosen for additional *in silico* investigation against both the wild-type and T790M mutant strain of EGFR and the wild-type HER2. The results reveal that certain substitution patterns increase the stability and assure stronger binding and higher H-bond occupancy of the conserved water molecule that is commonly observed with kinase crystal structures. Furthermore, the new inhibitor (T9) forms stable interactions with the mutant strain as a direct consequence of the enhanced ability to form additional hydrogen bonding interactions with binding site residues.



## 1. Introduction

Kinases are known to be a viable target for anti-cancer drug development [1–4]. It is estimated that approximately 30% of all drug design efforts are dedicated to the inhibition of kinases [5], which are the second most important drug targets after G protein-coupled receptors (GPCRs) [6]. Kinases are involved in many pathophysiological problems, especially cancers, in which their over-expression can lead to certain types of malignant tumors [7,8]. Several kinase inhibitors are now on the market, and many are undergoing clinical trials. However, resistance to current kinase inhibitors represents a significant issue; as a result, it is important to develop more effective approaches to resolving the problem of resistance [9]. In our previous studies, a new series of quinazoline-based lapatinib analogs with potential anti-tumor activity have been tested against Epidermal Growth Factor Receptors and Human Epidermal Growth Factor Receptors-2 tyrosine kinases (EGFR/HER2) [10,11]. Indeed, some members of the new series have shown micro-molar inhibitory activities and utilize new binding patterns [10,11]. In the present study, we continue our analysis to confirm the previous findings.

It is widely known that ligand binding to kinases is dominated mainly by vdW interactions [12,13]. In most cases, kinase inhibitors bind to the ATP (adenosine triphosphate) binding pocket of the kinase domain of the enzyme and form several hydrogen bonds (H-bonds) with the backbone and side chains of the amino acids that are present in this region (the Hinge region) [14]. Studies have shown that, for such receptors, ligand-induced polarization by protein environments can be important, and ligand binding is described appropriately by QM/MM (quantum mechanics/molecular mechanics) docking [15,16]. Our previous studies have shown that the vdW term might be a major factor that derives binding in this new series of inhibitors [10,11]. Primary QM/MM rescoring results have also been presented [10,11].

The ligand–protein binding process is too complex to be described by a single representation of the ligand–protein complex, which is produced as a result of docking [17]. Protein flexibility is increasingly important for appropriately describing the ligand–protein binding, especially for targets that are known to be highly flexible [18–20]. Kinases are known to be highly flexible and are a challenging target for docking [17,18]. In our previous studies, different docking and scoring methods that allow certain receptor

* Corresponding author. Tel.: +61 3 9214 8785.
** Corresponding author. Tel.: +61 3 9214 5065.
*E-mail addresses:* mmahmed@swin.edu.au (M. Ahmed), fwang@swin.edu.au (F. Wang).

1093-3263/$ – see front matter © 2013 Elsevier Inc. All rights reserved.
http://dx.doi.org/10.1016/j.jmgm.2013.06.004

flexibility have been used [10,11], such as rigid docking with vdW radii scaling [11], induced fit docking (IFD) and molecular dynamics (MD) simulations [10,11].

MD simulations for a sufficiently long time are important because certain conformational changes are not accessible at the conventional MD time scale. In the current study, we continue our attempt to find insights into the understanding of the binding of the new series to their targets, EGFR and HER2, which utilizes much longer MD simulations than studies that were conducted previously (10 ns) [10]. Another motivation is to *in silico* screen and assess the binding of a compound library of inhibitors with better binding and less liability to the problem of resistance, based on our previous findings [10,11]. The new series is compared with the originally co-crystallized ligands, lapatinib (EGFR) [21] and SYR (HER2) [22]. In addition, it is found that the new series interacts with certain additional residues in the binding site; further analysis of the interaction of the new series with some EGFR mutants, such as the famous T790M mutation [23,24], will provide useful insight. The T790M mutation, among others, is responsible for the development of resistance against lapatinib as well as other tyrosine kinase inhibitors (TKIs) [23,24]. Studies have shown that acquired lapatinib resistance due to the T790M (gate keeper) mutation is dominated by either severe steric clashes or disruption of the H-bonding network due to the surrounding water molecules [25–27]. Moreover, the T790M mutation was linked to an increased affinity to ATP, and only those inhibitors that have a covalent binding mode can still be effective [28].

The inhibitors M19 and M20 (Fig. 1) have been identified as the most active inhibitors among the series against EGFR and HER2 *in vitro* [10,11]. In the current study, the results of a primary *in silico* screening of a designed compound library of 200 inhibitors based on the M19 and M20 scaffolds are discussed. One of the most promising members of the *in silico* screened compound library, which is the T9 inhibitor, is subjected to additional extensive *in silico* investigation. The original co-crystalized inhibitors lapatinib (anti-EGFR, PDB code: 1XKK) [21] and SYR (anti-HER2, PDB code: 3PP0) [22] are considered to be references for the MD simulations. Some primary results for MD simulations of lapatinib, M19 and T9 against the T790M EGFR mutant are presented. In total, nine long MD simulations are conducted; (i) lapatinib, M19 and T9 with wild type EGFR (WT), and (ii) lapatinib, M19 and T9 with the T790 M mutant EGFR (MUT) and (iii) SYR, M19 and T9 with the wild type HER2 (WT). For simplicity, the wild type EGFR is denoted as EGFR (WT), and the mutant strain is denoted as EGFR (MUT). Wild type HER2 is denoted as HER2. In addition to MD simulations, binding free energy calculations are conducted based on either a single snapshot (Prime-MM/GBSA) or an ensemble of snapshots (AMBER-MM/PB(GB)SA). To account for the protein polarization effect, the relaxed MD complexes are rescored by QM/MM-based methods.

## 2. Methods and computational details

### 2.1. Design rationale

Fig. 1 represents the two dimensional (2D) chemical structures of lapatinib (a dually acting anti-EGFR/HER2 drug, Fig. 1a) and SYR (an HER2 inhibitor, Fig. 1b), erlotinib (anti-EGFR, Fig. 1c) and gefitinib (anti-EGFR, Fig. 1d), in addition to M19 (anti-EGFR/HER2, Fig. 1e) and M20 (anti-EGFR, Fig. 1f), which have been identified previously [10,11]. The 2D structure of the most active inhibitor of the newly designed library identified *in silico* (T9) is also given in Fig. 1e. The newly designed inhibitors benefit from the main skeleton of M19 in addition to substitutions at four different sites, at which the substitution is likely to give rise to more effective inhibitors.

The binding of the new series to either EGFR or HER2 is very similar, where the N1 atom of the quinazoline ring binds to Met793 (EGFR) or Met801 (HER2) [10,11], and the bulky 4-anilinoquinazoline side group binds to the side pocket formed by the displacement of the Cα-helix. The two terminal tails at positions $R_1$ and $R_2$ push the quinazoline ring for a better filling of the hinge region and also form lipophilic interactions with the nearby residues [10,11].

Because the vdW interaction term is the most important term in this class of receptors, the halogen atoms at positions $R_3$ and $R_4$ (—F, —Cl,—Br, —I, —CF3) become the primary focus. At the $R_1$ and $R_2$ positions, the chain length grows from one carbon (—methoxy) to three carbons (—propoxy). The lapatinib (Fig. 1a) [21] and erlotinib (Fig. 1c) [29] side chain tails, instead of the pure alkoxy group substituents, are also considered. Docking is conducted against the EGFR receptor (see below). The correctly docked inhibitors are given in the supplementary material. Note that this list also contains modifications for the second most active anti-EGFR ligand identified previously, *i.e.*, M20.

### 2.2. Ligand docking against EGFR

The details of the docking preparation and setup have been given previously [11]. Briefly, all of the ligands are docked against the EGFR crystal structure (PDB code: 1XKK) [21], using the same settings, and are ranked according to the XP_LipophilicEvdW term, as implemented in the extra-precision mode of the Glide docking software module of the Schrödinger suite (Glide XP) [30,31]. Only inhibitors that satisfy the presence of two predetermined H-bond constraints (with Met793 and the conserved water molecule) are kept. The XP_LipophilicEvdW term was able to give the highest correlation with the experimentally measured inhibitory activity ($r_{(\text{Pearson correlation})} = 0.78$ and $r^2 = 0.61$); as a result, it is the main selection criterion in the newly designed inhibitors [10,11]. The T9 inhibitor exhibits the highest XP_LipophilicEvdW score and is selected for more detailed computational investigation. The primary results suggest that T9 is able to form stronger interactions with both EGFR and HER2 than M19. T9 is also more capable than M19 of retaining the interactions with the conserved water molecules, which is observed in several crystal structures of kinases complexed with their corresponding inhibitors [32–35].

### 2.3. Molecular dynamics setup and binding energy calculations

The M19-protein complexes obtained from the previous IFD (HER2) [10] and rigid (EGFR) [11] runs are used for the MD simulations. The T9-HER2 complex is produced by mutating the M19 inhibitor in the M19-HER2 complex obtained previously using the IFD protocol [10]. This step is followed by a quick relaxation with Macromodel [36] to remove steric clashes. The T9-EGFR complex is obtained from the current docking run. For the lapatinib-EGFR (PDB code: 1XKK, hereafter will be denoted as lapa-EGFR) [21] and the SYR-HER2 (PDB code: 3PP0) [22] complexes, the original crystal structures are used. The structure preparation and the following MD simulations are performed using the AMBER12 software package [37], applying the ff03 force field [38,39]. Single point calculations of the corresponding inhibitors are performed at the B3LYP/cc-pVTZ level of theory in ether ($\varepsilon = 4.2$) solvent, applying the IEF-PCM model [40] and using the Gaussian 09 program [41]. The inhibitor charges and other parameters are obtained using the RESP fitting [42] procedures and the general AMBER force field (GAFF) [43]. The complexes are then solvated with a box of TIP3P [44] water with a buffer size of 15 Å and are neutralized by counter ions.

Each system is then subjected to four consecutive minimization steps. In each step, water molecules and ions are allowed to move

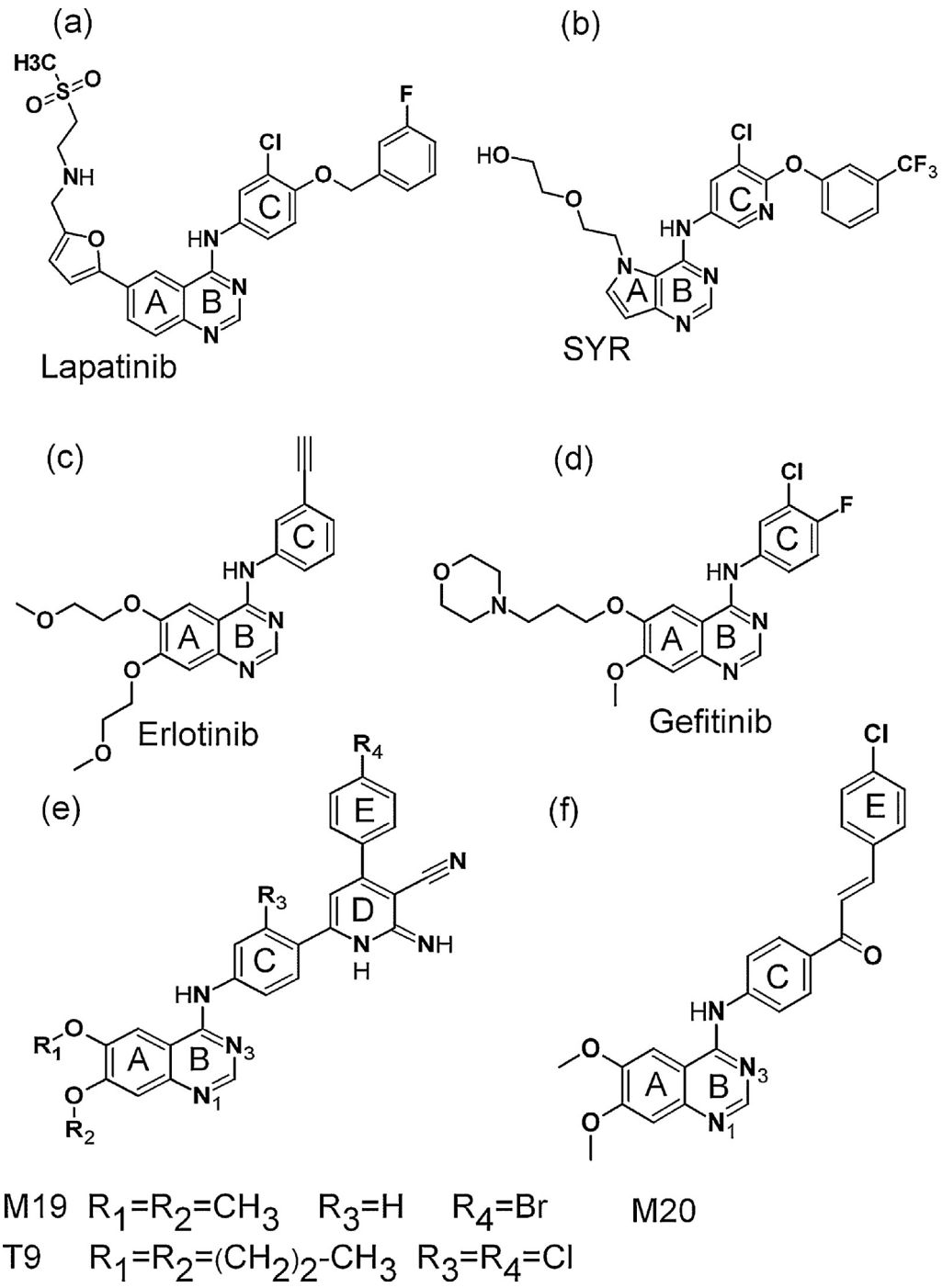


**Fig. 1.** The two-dimensional (2D) chemical structures of some approved tyrosine kinase inhibitors and the compounds under study.

freely for 1000 steps of steepest descent minimization followed by 4000 steps of conjugate gradient minimization. During minimization, protein and inhibitor atoms are constrained to their original positions by a force constant of 100 kcal mol$^{-1}$ Å$^{-2}$; then, there is a gradual relief of the force constraints to 50, 5 and zero (no constraints) kcal mol$^{-1}$ Å$^{-2}$, respectively. Following minimization, two consecutive steps of heating and equilibration are performed. First, each system is gradually heated in the NVT ensemble from 0 K to 300 K for 30 ps, with a time step of 1 fs, applying a force constant of 10 kcal mol$^{-1}$ Å$^{-2}$ on the protein and inhibitor coordinates. Langevin dynamics with the collision frequency $\gamma$ of 1 ps$^{-1}$ for temperature control is employed. A further 1 ns simulation in the NPT ensemble is performed to equilibrate the system density while applying a time step of 2 fs, which requires the use of the SHAKE algorithm [45] to constrain all of the bonds that involve hydrogen atoms. The temperature is controlled using Langevin dynamics with the collision frequency $\gamma$ of 1 ps$^{-1}$ and is maintained at 300 K. The pressure is maintained at 1 bar by applying a Berendsen barostat with a pressure relaxation time of 1 ps. Each system is again relaxed in the NVT ensemble for another 2 ns. In the first 1 ns, heavy atoms are constrained by a force constant of 10 kcal mol$^{-1}$ Å$^{-2}$. Each system is then subjected to a 10 ns "warming up" simulation, followed by 4 production simulations of 20 ns long each, *i.e.*, 80($4 \times 20$) ns in total, applying the NVT ensemble at 300 K and using Berendsen temperature control [46]. In all of the simulation steps, long-range electrostatics are computed using the particle mesh Ewald (PME)

[47] with a non-bonded cut-off of 12 Å. The edge effect is removed by applying periodic boundary conditions. All of the MD simulations were run using the PMEMD module of AMBER12 [37]. The binding energies were calculated from the MD trajectories using the PBSA module in AMBER12 [48].

For complexes that are subjected to MD simulations, physics-based rescoring is conducted by applying both the MM and QM/MM techniques. For MM rescoring, a single end point rescoring for the final trajectory snapshot produced from the MD simulations and using the Prime/MM-GBSA code of the Schrodinger suite [49–51] was employed. The complexes were also rescored applying the sophisticated AMBER/GB(PB)SA module in AMBER12 [48]. The AMBER/GB(PB)SA module takes advantage of statistical averaging over many potential configurations. Every second frame of the produced 8000 frames is selected, *i.e.*, a total of 4000 simulation snapshots are utilized. For QM/MM binding energy estimation, the AMBER QM/MM-GBSA calculations are utilized, and the QM subsystem is extended to the ligand in addition to the surrounding residues within 5 Å from the ligand. The dispersion-corrected AM1 (AM1-D) [52,53] Hamiltonian is utilized for the QM subsystem; for the MM subsystem, the ff03 force field is used [38]. The AM1 model is especially widely used in QM/MM ligand–protein binding energy calculations and QM/MM molecular dynamics simulations and gives very good results at a reasonable computational cost [54–56].

## 3. Results and discussion

Almost all of the tyrosine kinase inhibitors (TKIs) are either competitive or non-competitive inhibitors for the evolutionarily conserved ATP binding site of the tyrosine kinase systems, EGFR and HER2 [14,57,58]. This ATP binding site is located in a deep cleft that connects the N-lobe and the C-lobe and is conventionally known as the "Hinge region" [14,57,58]. Due to their high flexibility, available X-ray crystal structures of kinases complexed with their inhibitors show a high level of diversity with respect to the molecular structure of the inhibitors [59]. This high flexibility imposes challenges to the molecular modeling process. There are several methods for the classification of TKIs [60–62]. Briefly speaking, TKIs are classified into three main classes. The first class of inhibitors target either the active (DFG-in) or the inactive (DFG-out) state of the protein [21,63]. The second class of inhibitors target the (DFG-in) state in addition to a selectivity pocket that is formed as a result of a large shift of the Cα-helix; this Cα-helix shifted conformation represents an inactive state of the protein [62]. This large shift creates a deep pocket in the back of the protein by giving more room to accommodate bulky groups in the corresponding inhibitors. The third class of inhibitors can bind the ATP pocket and nearby allosteric sites [62,64]. An example from the first class is gefitinib (Iressa®, Fig. 1d), which can bind the active (DFG-in) state of the protein [65,66]. This inhibitor is characterized by the presence of a small side group at the 4-anilino site. An example of the second class is lapatinib (Tykerb®, Fig. 1a) [67,68]. In contrast, to gefitinib, lapatinib possesses a bulkier group at the 4-anilino site. This bulky group is accommodated by a deep pocket that is created as a result of a large shift in the Cα-helix [21,63]. The recently released X-ray crystal structure of HER2 complexed with the inhibitor (SYR, Fig. 1b) [22] shows that SYR binds to an active-like conformation of the HER2 receptor. Previous modeling studies for HER2 have utilized homology modeling and used EGFR as a template due to its high sequence similarity to HER2 (81%) [26,27].

In general, inhibitor binding to either EGFR or HER2 is driven by strong vdW forces in addition to a strong H-bond with a conserved Met residue at the hinge region through the N1 atom of the quinazoline ring. Other studies have identified the importance of the conserved water molecule that is typically observed in many crystal structures of kinases that are co-crystalized with their corresponding ligands [32,34,69–71]. However, experiments show that this water molecule is not essential for the inhibitory effect, and some active inhibitors that were previously reported lack the N atom at position 3 (N3) that is responsible for the interaction with this water molecule [29,72]. In certain cases, an extra cyano group at this site reduces the need for this N3 atom *via* direct interaction with the nearby Thr residue [73,74].

### 3.1. Docking and scoring

Table 1 reports the XP_Gscore and the XP_LipophilicEvdW docking scores of the 10 most active *in silico* designed inhibitors together with the substitution groups at $R_1$, $R_2$, $R_3$ and $R_4$. It has been shown that the hit structure M19 is the top active inhibitor against both EGFR ($IC_{50}$ = 1.935 μM) and HER2 ($IC_{50}$ = 1.035 μM) [10,11]. In this section, only EGFR is considered for discussion as a result of data transferability that originates from high sequence similarity (81%). Additionally, the discussion is limited to the M19 modifications because M19 is a dually acting inhibitor, whereas M20 shows a very weak anti-HER2 inhibitory effect ($IC_{50}$ against EGFR: 2.582 μM and against HER2 99.96 μM) [10,11]. The XP_LipophilicEvdW score, which qualitatively identified the top active anti-EGFR, is employed for inhibitor selection in the present docking study. The derivatives are given in the table according to this score.

As shown in Table 1, all of the modifications show a higher XP_LipophilicEvdW score than the hit structure M19. Interestingly, pure alkoxy substituents at the $R_1$ and $R_2$ positions are more favored than hetero substituted alkyl groups, such as the ethoxy-methoxy group present in erlotinib (as in T8e with a XP_LipophilicEvdW score of -9.28 and T11e with a XP_LipophilicEvdW score of -9.20) or the substituted Furyl group that is present in lapatinib (as in T12l with an XP_LipophilicEvdW score of −8.96). It is not the intention of this study to test the electron withdrawing groups (EWGs) at these two sites ($R_1$ and $R_2$), because previous studies have shown that EWGs at these two sites of the 4-anilinoquinazoline scaffold tend to decrease the antitumor activity significantly [75,76]. Additionally, optimal activity is achieved with chlorination at the $R_3$ and $R_4$ positions, which is also found in the case of T9 (XP_LipophilicEvdW score of -9.40).

## 4. Molecular dynamic simulations

### 4.1. General binding remarks

Fig. 2 represents the root mean square deviations (RMSDs) of the Cα atoms for the nine complexes under study through the 80 ns production simulations. These complexes are the T9, M19 and lapatinib with EGFR(WT) and EGFR(MUT) receptors, respectively, and T9, M19 and SYR with the HER2 receptor. As shown in the figures, the inhibitor–protein complexes show overall reasonable RMSD values. Small discrepancies are expected as a result of the known flexibility of kinases. As mentioned before, TKIs bind to the ATP binding site of both EGFR and/or HER2 receptors, and the binding is dominated by vdW interactions. An essential requirement for binding is the presence of a nitrogen atom at position 1 of the heterocyclic ring (N1). This heterocyclic ring might be a quinoline, quinazoline, pyridopyrimidine or even a mono-cyclic ring [77]. This nitrogen binds strongly to a Met residue at the hinge region (Met793 in EGFR and Met801 in HER2), and derivatives without this N atom are almost inactive [76,77]. Nitrogen substitution at position 3 (N3) ensures the binding to a water molecule that is observed frequently in kinase crystal structures [32–35]. This water molecule forms a bridge (through H-bonds) between the N3 of the

**Table 1**
R group modifications of the *in silico* designed compounds library against the EGFR receptortogether with the docking scores.

| Title | Substituents | | | | XP GScore | XP_LipophilicEvdW | %inhibition[a] | $IC_{50}$ (μM)[a] |
|---|---|---|---|---|---|---|---|---|
| | $R_1$ | $R_2$ | $R_3$ | $R_4$ | | | | |
| | 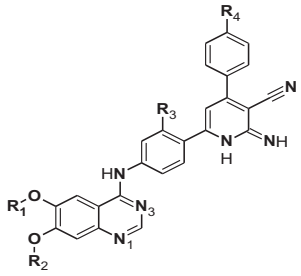 | | | | | | | |
| T9 | —$(CH_2)_2$—$CH_3$ | —$(CH_2)_2$—$CH_3$ | —Cl | —Cl | −9.02 | −9.40 | | |
| T16 | —$(CH_2)_2$—$CH_3$ | —$(CH_2)_2$—$CH_3$ | —Cl | —$CF_3$ | −8.88 | −9.39 | | |
| T11 | —$(CH_2)_2$—$CH_3$ | —$(CH_2)_2$—$CH_3$ | —Br | —Br | −8.89 | −9.38 | | |
| T1 | —$(CH_2)_2$—$CH_3$ | —$(CH_2)_2$—$CH_3$ | —Cl | —Br | −8.92 | −9.33 | | |
| T8e | —$(CH_2)_2$—O—$CH_3$ | —$(CH_2)_2$—O—$CH_3$ | —Br | —Cl | −8.62 | −9.28 | | |
| T11e | —$(CH_2)_2$—O—$CH_3$ | —$(CH_2)_2$—O—$CH_3$ | —Br | —Br | −8.74 | −9.20 | | |
| T12 | —$(CH_2)_2$—$CH_3$ | —$(CH_2)_2$—$CH_3$ | —F | —Br | −10.05 | −9.20 | | |
| T3 | —$(CH_2)_2$—$CH_3$ | —$(CH_2)_2$—$CH_3$ | —Cl | —F | −9.03 | −9.18 | | |
| T8 | —$(CH_2)_2$—$CH_3$ | —$(CH_2)_2$—$CH_3$ | —Br | —Cl | −11.33 | −8.99 | | |
| T12l | 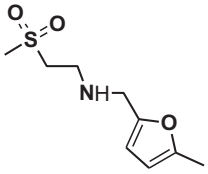 | —H | —F | —Br | −7.76 | −8.96 | | |
| M19 | —$CH_3$ | —$CH_3$ | —H | —Br | −10.78 | −8.40 | 72 | 1.935 |

[a] At a 5 μM concentration; see Ref. [10,11].

inhibitor and nearby residue side chains, such as Cys and Thr. Fig. 3 shows the potential locations of three hydration sites (S1, S2 and S3) around the inhibitors under study. As shown in Fig. 3, the water molecule at the S1 site, together with other water molecules, forms a network of H-bonds around the inhibitor. Although such a water molecule is not essential for the anti-EGFR and/or anti-HER2 activities, recent studies link some binding problems against kinases to the disruption of such favoring interactions [12,27]. Another two potential sites for the presence of water molecules are the S2 site, in which water molecules bind to the aniline hydrogen, and the S3 site, which is linked to the nearby Gln amino acid.

### 4.2. Water molecule occupancies

Analysis of the MD trajectories shows that the H-bond occupancies of the S1, S2 and S3 sites are different for different inhibitor-protein complexes. Fig. 3 presents the locations of these three sites (S1, S2 and S3) around the inhibitors under study. Table 2 represents the % occupancy of the potential water-mediated H-bonds as a function of the simulation time. In all of the cases, an upper distance cut-off of 3.5 Å and a lower angle cut-off of 120° are used for the H-bonds. Because there is a possibility for the two hydrogens of the same water molecule or more than one water

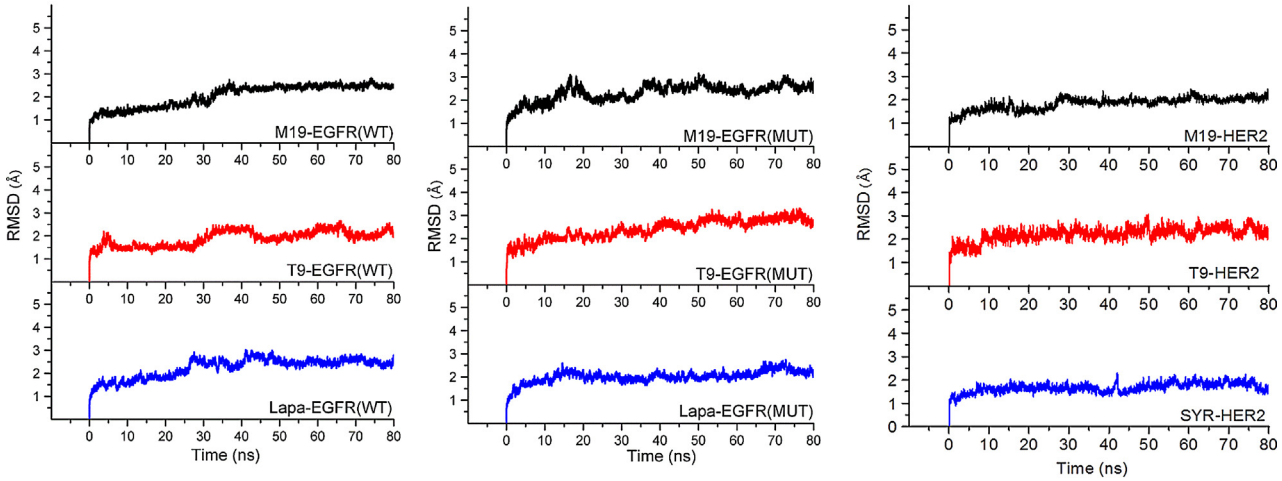


**Fig. 2.** Cα backbone atoms RMSD plots for the studied complex during the 80 ns MD simulations. M19 complexes are black colored, T9 complexes are red colored and lapatinib complexes are blue colored. Left panel is for EGFR(WT) complexes, middle panel is for EGFR(MUT) complexes and right panel is for HER2 complexes.

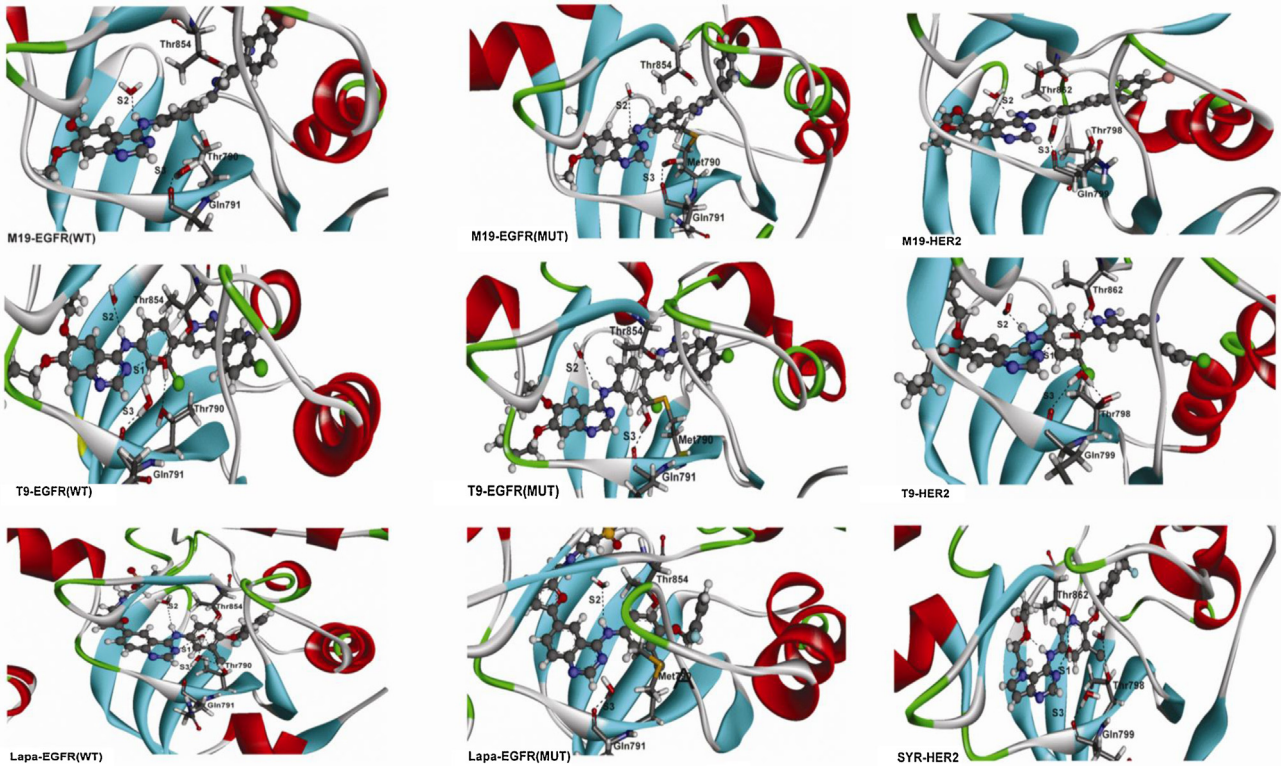


**Fig. 3.** Potential binding poses and water orientation of the 9 studied complexes. Left panel is for EGFR(WT) complexes, middle panel is for EGFR(MUT) complexes and right panel is for HER2 complexes.

molecule to interact simultaneously with the same site, it is possible that the occupancy could exceed 100%.

In all of the situations, the most conserved occupancy site is observed at the S3 site. The T9-HER2 complex achieves the highest value of 123.54% of the simulation period for this site (S3). However, because the occupant water molecules at this site (S3) do not directly interact with the inhibitor, this S3 site might have the least influence in comparison with the S1 and S2 sites. It should be stressed here that neither of these water molecules exist in the original crystal structures nor are they constrained to their 3D coordinates. For the S2 site, the % occupancy values for all of the complexes are comparable, with the exception of the SYR-HER2 complex, which exhibits Zero % occupancy at this site; this level of occupancy could be due to the potential formation of an intramolecular H-bond. In addition, the highest % occupancy for the S2 site is exhibited by the lapa-EGFR(WT) complex, which is given by 94.77%, followed by that for T9-EGFR(WT), which is given by 85.54%. For the EGFR(MUT) complexes. T9 exhibits the highest occupancy, with a value of 70.09%, which is followed by M19 (69.25%) and, finally, lapatinib (60.84%).

The most interesting water % occupancy is observed with the S1 site. The highest occupancy is achieved with SYR-HER2, with a % occupancy of 97.54%, followed by lapa-EGFR (WT), with a value of 94.5%. For the new inhibitors, both the hit (M19) and the optimized structure (T9) show interesting behavior. M19 completely lacks such interactions in all situations, having a maximum value of 1.71% for its complex with EGFR (WT). Such low occupancy values can be considered essentially insignificant. In contrast to M19, the new inhibitor T9 exhibits a much higher occupancy at the S1 site, of approximately 91.05% with HER2, and a value of 70.03% with EGFR (WT). As a result of the increased hydrophobicity around the S1 site due to the T790M mutation, water occupancy at this site is significantly reduced from 94.50% in lapa-EGFR (WT) to 28.69% in lapa-EGFR (MUT) and from 70.03% in T9-EGFR (WT) to Zero % in T9-EGFR (MUT).

The literature shows that almost all of the effective anilinoquinazoline EGFR and/or HER2 competitive inhibitors, especially the currently marketed inhibitors, are substituted at ring **"C"**, mostly with electron-withdrawing groups, such as halogen (gefitinib and lapatinib, Fig. 1) and/or ethyne (erlotinib, Fig. 1) groups

**Table 2**
% Hydrogen-bond occupancy analysis of the three observed water sites as a function of the simulation time.

| Inhibitor-EGFR (WT) | | | Inhibitor-EGFR (MUT) | | | Inhibitor-HER2 (WT) | | |
|---|---|---|---|---|---|---|---|---|
| M19 | S1 | 1.71 | M19 | S1 | 1.10 | M19 | S1 | 0.11 |
| | S2 | 41.61 | | S2 | 69.25 | | S2 | 58.20 |
| | S3 | 61.09 | | S3 | 78.14 | | S3 | 111.48 |
| T9 | S1 | 70.03 | T9 | S1 | Zero | T9 | S1 | 91.05 |
| | S2 | 85.54 | | S2 | 70.09 | | S2 | 67.44 |
| | S3 | 89.89 | | S3 | 91.80 | | S3 | 123.54 |
| Lapatinib | S1 | 94.50 | Lapatinib | S1 | 28.69 | SYR | S1 | 97.54 |
| | S2 | 94.77 | | S2 | 60.84 | | S2 | Zero |
| | S3 | 114.90 | | S3 | 69.14 | | S3 | 113.65 |

[72,75,78]. In the new series, the modified T9 shows such substitutions. Primary results suggest that the substitution of ring "**C**" by a halogen can affect the stability of the complex and the binding to the conserved water molecule, and this finding might be due to steric reasons. For example, as shown in Fig. 3, because of the existence of different rotameric conformations of the side chains of nearby residues that are responsible for binding to this bridging water molecule at the S1 site, *i.e.*, Thr790 and Thr854, such an interaction is possible in lapatinib and T9 but is unlikely in M19. For the same reasons, for inhibitor-HER2 complexes, the presence of different rotameric structures of Thr798 and Thr862 are responsible for the existence of high water occupancy at the S1 site for SYR (97.54%) and T9 (91.05%) but as low as 0.11% for M19. Systematic study to reveal this effect is currently in progress.

### 4.3. Binding to the conventional hinge residues

Inhibitor binding to both EGFR and HER2 is dominated by vdW interactions. The strength of this binding can be *in silico* assessed by calculating the binding energy as well as the stability of the formed complexes. For the inhibitors that are under study, all can interact with the conserved hinge Met residue (*i.e.*, Met793 for EGFR and Met801 for HER2). Studies have shown that, for the EGFR receptors, acquired resistance due to the T790M mutation prevents stable interaction with competitive inhibitors, including lapatinib [26]. This finding has been attributed to several reasons: (i) steric clashes, (ii) disruption of the surrounding water-mediated H-bonds and (iii) increased sensitivity to ATP [26,27]. Indeed, the present study shows that the surrounding water-mediated H-bond network is severely disrupted in the case of the T790M mutation. This disruption of the water-mediated interaction, in addition to the other reasons, causes the anti-tumor activity of lapatinib against EGFR to be severely decreased from EGFR (WT) (with an $IC_{50}$ of 0.022 μM) to EGFR (MUT) (with an $IC_{50}$ of 3.3 μM) [26].

Fig. 4 shows the fluctuation of the inhibitor@N1···Met793 (EGFR) or the inhibitor@N1···Met801 (HER2) H-bond during the 80 ns simulation period. This H-bond is the most important anchor, and inhibitors that lack such an H-bond are inactive. In all of the cases, the fluctuation is minimal, and this H-bond can be considered to be very stable. An exception is the lapatinib complex with the EGFR (MUT), in which a larger fluctuation appears after approximately 60 ns–5 Å. This finding could shed some light on the possible instability of the lapatinib-EGFR (MUT) complex. However, a complete ligand escape during the conventional simulation time for EGFR (MUT) is not expected, given the limitations of the current modeling tools and the complicated energy landscape, as discussed before for gefitinib binding to the EGFR T790 M mutant [79]. In all complexes, the average value of this H-bond range is ~2–2.5 Å.

### 4.4. Binding to the additional hinge residues

The ability of the new inhibitors to bind to additional hinge residues in both the EGFR and HER2 binding sites have been discussed before [10,11]. Due to the high sequence similarity between the EGFR and HER2 receptors, the locations of such interactions are similar [10,11]. In general, the most important interactions are the two charge-assisted H-bonds that formed with Asp855 and Lys745 (EGFR) or Asp863 and Lys753 (HER2). They are mediated by the N—H group of ring "**D**" and the extra imino group on the same ring, respectively. Because of structural reasons, neither SYR nor lapatinib can form such charge-assisted interactions. However, the possible interaction between SYR and Asp863 is *via* the terminal hydroxyl group at the other side of the molecule. This interaction is indeed observed in the crystal structure itself and is formed during the simulation. Fig. 5 displays the interaction of T9 and M19 with the three receptor types, EGFR (WT), EGFR (MUT) and HER2. Because such a static representation is not sufficient due to the lack of dynamic information, Table 3 reports the % occupancies of such interactions as a function of the simulation time. As shown in the table, the most stable interactions are the T9-Asp863(HER2) and the M19-Lys753(HER2) interactions, which have an occupancy of 71.03% and 66.86%, respectively. The new inhibitor T9 maintains a higher % occupancy for the interactions with EGFR (MUT) than the corresponding interaction with EGFR (WT). In addition, the occupancy of the M19 interaction with Lys745-EGFR (MUT) is given by 66.2%, whereas its interaction with Lys745-EGFR (WT) is given by 41.96%. In contrast to the M19 interaction with Lys745, which is higher in EGFR (MUT) than in EGFR (WT), the occupancy of the M19 H-bond interaction with Asp855 is significantly higher in EGFR (WT) (12.51%) than in EGFR (MUT) (1.78%). Occasionally, M19 can form an H-bond with the amide oxygen of Asp863 in HER2.

This demonstrated ability of the new inhibitors to bind to these extra residues is a preferred property. Some of the very challenging mutations that result in resistance to the current EGFR/HER2 are those that are present in the vicinity of the hinge region. An example of such mutations is the stubborn T790M mutation, which is known to be present in more than 50% of all of the patients whose tumors showed an acquired resistance to TKIs [80,81]. The formation of very strong interactions with additional residues could retain the antitumor activity in the EGFR/HER2 mutant strains, including the T790M mutation. Although it has been shown that irreversible inhibitors could be the agents of choice for the resistant strains, toxicity concerns might be a problem for these agents [25,82,83].

## 5. Binding energy calculations

### 5.1. Total binding energy

Table 4 reports the binding energy scores for the inhibitors at different QM/MM and pure-MM levels of theory. The binding energies are given in negative values, and the more negative the value is, the higher the binding energy. In general, MM-based methods produce compatible results with the QM/MM-based methods. T9 exhibits higher binding energy scores than M19 in all of the situations. The introduction of the conserved water molecule enhances the overall binding scores and especially the electrostatic ($\Delta E_{ele}$) term, which will be discussed in the following section. A direct comparison between the binding energy scores for ligands that have different scaffolds should be conducted with caution due to different entropic terms and dissociation rates.

Overall, lapatinib shows higher binding energy ($\Delta G$) for the mutant (MUT) rather than the wild-type (WT) strain of EGFR, which is against the experimental $IC_{50}$ trend reported in Table 4 [26]. The previously calculated $\Delta G$ value for lapa-EGFR(MUT) and lapa-EGFR(WT) complexes are given by $-63.28\ kcal\ mol^{-1}$ and $-62.19\ kcal\ mol^{-1}$, respectively, without considering the water molecule at the S1 site [27]. However, inclusion of the water molecule slightly enhanced the lapa-EGFR(WT) binding energy ($\Delta G$) by approximately $2.56\ kcal\ mol^{-1}$ over the lapa-EGFR(MUT) complex [27]. In principle, this behavior might be related to certain inadequacies in MMPB(GB)SA parameterization as shown by other studies [84,85]. Moreover, caution must be taken when analysis of binding energies, as the lapa-EGFR(MUT) is a virtual complex which should not present in reality and very long simulation may result in complete ligand escape.

For the other complexes, it is noted that only the dispersion-corrected AM1 Hamiltonian (AM1-D) predicts M19 to be a better binder for HER2 ($-162.85\ kcal\ mol^{-1}$) than EGFR ($-133.60\ kcal\ mol^{-1}$). This finding is consistent with the experimentally measured $IC_{50}$ for M19 against HER2 (1.035 μM) and EGFR (1.935 μM) [10,11]. AM1-D binding energy estimation includes all

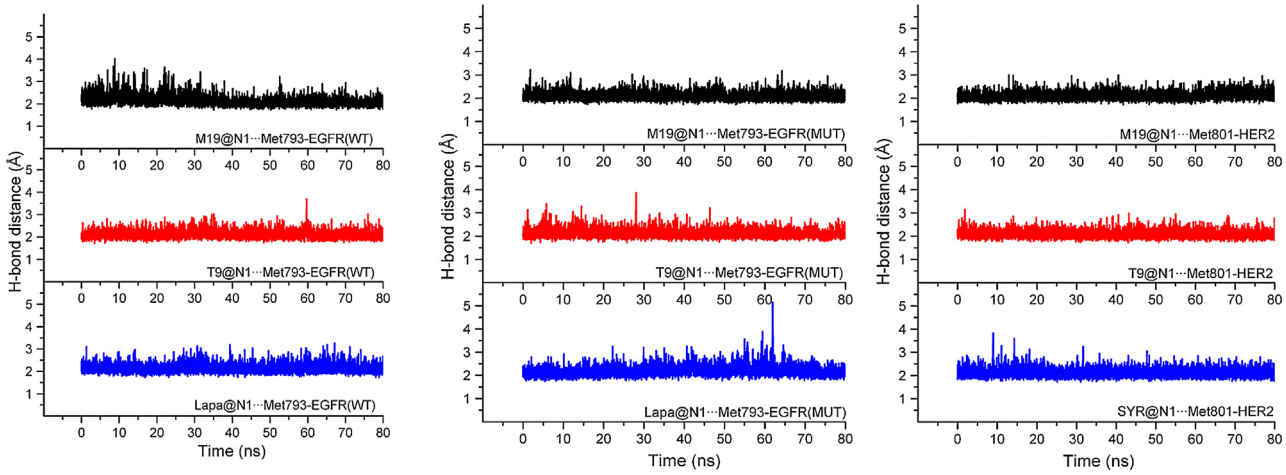


**Fig. 4.** Hydrogen bond distance profiles between the inhibitors (M19, T9 and lapatinib)@N1and the Met hinge residue (Met793 in EGFR and Met801 in HER2) during the 80 ns MD simulation. M19 complexes are black colored, T9 complexes are red colored and lapatinib complexes are blue colored. Left panel is for EGFR(WT) complexes, middle panel is for EGFR(MUT) complexes and right panel is for HER2 complexes. (For interpretation of references to color in this figure legend, the reader is referred to the web version of this article.)

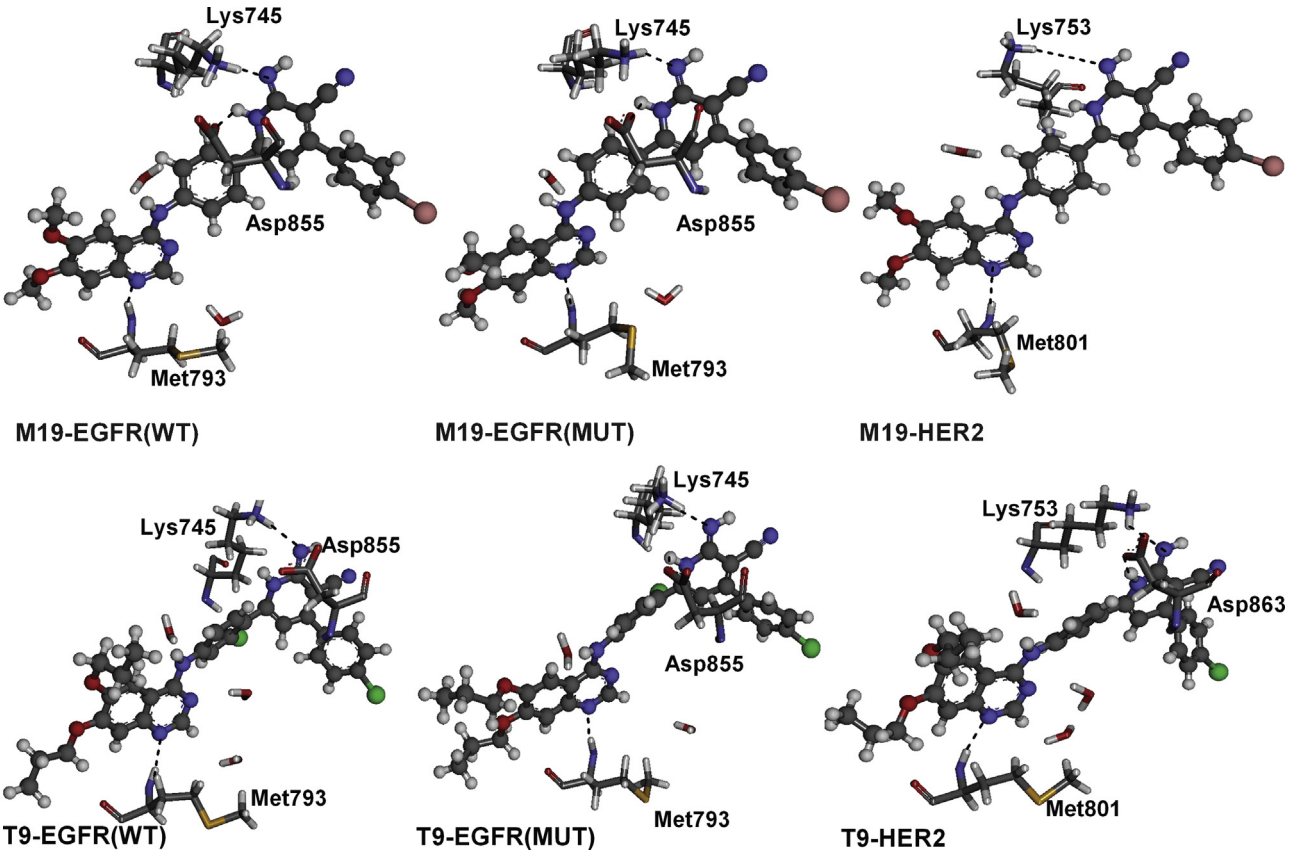


**Fig. 5.** The three-dimensional (3D) interactions of T9 and M19 with the conserved hinge region Met residue and the additional residues Asp and Lys of EGFR (WT), EGFR (MUT) and HER2. Left panel is for EGFR(WT) complexes, middle panel is for EGFR(MUT) complexes and right panel is for HER2 complexes.

**Table 3**
% Hydrogen-bond occupancy analysis of the additional potential hinge residue interactions.

| Inhibitor-EGFR(WT) | | | Inhibitor-EGFR(MUT) | | | Inhibitor-HER2(WT) | | |
|---|---|---|---|---|---|---|---|---|
| M19 | Asp855 | 12.51 | M19 | Asp855 | 1.78 | M19 | Asp863 | Zero |
| | Lys745 | 41.96 | | Lys745 | 66.2 | | Lys753 | 66.86 |
| T9 | Asp855 | 14.49 | T9 | Asp855 | 66.51 | T9 | Asp863 | 71.03 |
| | Lys745 | 13.02 | | Lys745 | 31.84 | | Lys753 | 56.92 |

**Table 4**
Experimental % inhibition together with simulated binding energies and scores for the MD-produced complexes (kcal·mol$^{-1}$).

| Title | AMBER-QM-MM/GBSA[a] | Prime-MM/GBSA[b] | AMBER-MM/GBSA[c] | AMBER-MM/PBSA[c] | $IC_{50}$ (μM) | %Inhibition[d] |
|---|---|---|---|---|---|---|
| **EGFR (WT)** | | | | | | |
| M19 | −133.60 | −136.14 | −65.63 | −95.29 | 1.935[e] | 72 |
| T9 | −139.86 | −152.83 | −69.95 (−73.58) | −103.44 (−108.46) | | |
| Lapatinib | −91.16 | −128.37 | −68.12 (−71.74) | −99.93 (−103.57) | 0.022[f] | |
| **EGFR (MUT)** | | | | | | |
| M19 | −121.18 | −130.75 | −61.83 | −92.18 | | |
| T9 | −139.06 | −153.56 | −70.45 | −102.07 | | |
| Lapatinib | −96.38 | −142.36 | −75.16 | −105.62 | >3.3[f] | |
| **HER2** | | | | | | |
| M19 | −162.85 | −116.14 | −59.34 | −93.34 | 1.035[e] | 85 |
| T9 | −164.23 | −159.58 | −66.28 (−69.04) | −100.38 (−104.36) | | |
| SYR | −77.73 | −136.64 | −62.38 (−66.31) | −91.36 (−96.02) | 0.011[g] | |

[a] QM system composed of ligand and the nearby residues within 5 Å; the QM system was treated with the dispersion-corrected AM1 Hamiltonian (AM1-D), and the MM system was treated with the AMBER-ff03 force field.
[b] Residues within 6 Å of the inhibitor are treated flexibly.
[c] Values between brackets are those obtained upon inclusion of the conserved water molecule (S1) in the calculation.
[d] At a 5 μM concentration, see Ref. [10,11].
[e] See Ref. [10,11].
[f] See Ref.[26].
[g] See Ref. [22].

of the surrounding residues within 5 Å of the inhibitor in the QM subsystem. It should also be noted that other binding energy scores depend on the modeling techniques and theory levels that are employed.

### 5.2. Component contributions to the total binding energy

To further elucidate and assess the contributions of the binding energy components to the total binding energy, Table 5 reports the individual binding energy components that were calculated using the AMBER/MM-PBSA tool. The total binding energies receive contributions from the $\Delta E_{vdW}$ and $\Delta E_{ele}$ components. In Table 5, the binding energies can be considered to be "gas phase" binding energies because they do not include the desolvation penalties. The binding energy components of the inhibitor-EGFR(MUT) complexes are not considered in this section.

As shown in the table and in all of the complexes, the $\Delta E_{vdW}$ term is the dominant component. For the EGFR (WT) complexes, the T9 complex shows an enhanced $\Delta E_{vdW}$ component, which is given by −83.09 kcal mol$^{-1}$ compared to the same term for M19 (−75.99 kcal mol$^{-1}$) and lapatinib (−76.42 kcal mol$^{-1}$). For the $\Delta E_{ele}$ binding energy component, T9 exhibits an enhanced contribution, which is given by −31.57 kcal mol$^{-1}$ compared to M19 (−24.20 kcal mol$^{-1}$) and lapatinib (−29.16 kcal mol$^{-1}$).

**Table 5**
Decomposed binding energies of the complexes studied with MD (kcal·mol$^{-1}$).

| Title | $\Delta E_{vdW}$[a] | $\Delta E_{ele}$[a] | $\Delta E_{tot(vdW+ele)}$[a] |
|---|---|---|---|
| **EGFR(WT)** | | | |
| M19 | −75.99 | −24.20 | −100.19 |
| T9 | −83.09(−84.07) | −31.57(−35.06) | −114.66(−119.13) |
| Lapatinib | −76.42(−77.15) | −29.16(−33.38) | −105.58(−110.53) |
| **EGFR(MUT)** | | | |
| M19 | −73.27 | −22.27 | −95.54 |
| T9 | −81.23 | −26.46 | −107.69 |
| Lapatinib | −85.88 | −39.15 | −125.03 |
| **HER2** | | | |
| M19 | −70.56 | −26.75 | −97.31 |
| T9 | −76.19(−76.96) | −20.23(−23.63) | −96.42(−100.59) |
| SYR | −68.27(−68.69) | −24.59(−29.99) | −92.86(−98.68) |

[a] Values between brackets are those obtained upon inclusion of the conserved water molecule (S1) in the calculation.

Interestingly, inclusion of the conserved water molecule (S1) through the 1WAT protocol (*i.e.*, only water at the S1 site is considered) contributes to the $\Delta E_{ele}$ term, without having obvious effects on the $\Delta E_{vdW}$ term. This inclusion results in an energy gain for the $\Delta E_{ele}$ term of 3.49 kcal mol$^{-1}$ and 4.22 kcal mol$^{-1}$ for T9 and lapatinib, respectively. This calculation is in agreement with the reported literature values for the inclusion of such water molecules (∼3.5–3.6 kcal mol$^{-1}$) [27].

For the HER2 complexes, T9 shows the largest contribution from the $\Delta E_{vdW}$ term, which is given by −76.19 kcal mol$^{-1}$ compared to M19 (−70.56 kcal mol$^{-1}$) or SYR (−68.27 kcal mol$^{-1}$). The $\Delta E_{ele}$ term for SYR is enhanced by the introduction of the water molecule ($\Delta\Delta E_{ele}$ = 5.4 kcal mol$^{-1}$), in contrast to the gain for T9 ($\Delta\Delta E_{ele}$ = 3.4 kcal mol$^{-1}$).

### 5.3. Per-residue binding energy decomposition

Per-residue binding energy decomposition analysis is important for understanding the important residues that favor the binding; thus, individual binding energy components on per-residue decomposition analysis are shown in Fig. 6. Only the most important residues are shown in the figure. Selection is based primarily on the residue contributions to the $\Delta E_{vdW}$ term for the new inhibitors, T9 and M19. The labels in the figure represent the exact binding contributions of each selected amino acid to the corresponding term. As shown in the figure, Asp855(863) and Lys745(753) have large contributions to the binding energy for the $\Delta E_{vdW}$ and $\Delta E_{ele}$ terms. In addition, in all of the complexes, T9 exhibits the largest contribution from Met793(801), which can be considered to be the most important anchoring point.

For the EGFR (WT) complexes, the Asp855 contribution to the $\Delta E_{vdW}$ term is higher in M19 (−3.48 kcal mol$^{-1}$) than in T9 (−3.35 kcal mol$^{-1}$). On the other hand, the Lys745 contribution is larger for T9 (−2.28 kcal mol$^{-1}$) than for M19 (−1.27 kcal mol$^{-1}$) for the same term ($\Delta E_{vdW}$). The discrepancies between T9 and M19 for the $\Delta E_{ele}$ term with respect to these two amino acid residues are not directly correlated with the H-bond occupancies (Table 3). This finding is evidenced by the slightly large $\Delta E_{ele}$ contribution of the Asp855 residues in the lapatinib binding, although lapatinib does not form a direct specific H-bond interaction with this residue.

For the EGFR (MUT) complexes, T9 and M19 possess larger contributions from Asp855 to the $\Delta E_{vdW}$ term (−2.52 kcal mol$^{-1}$ and

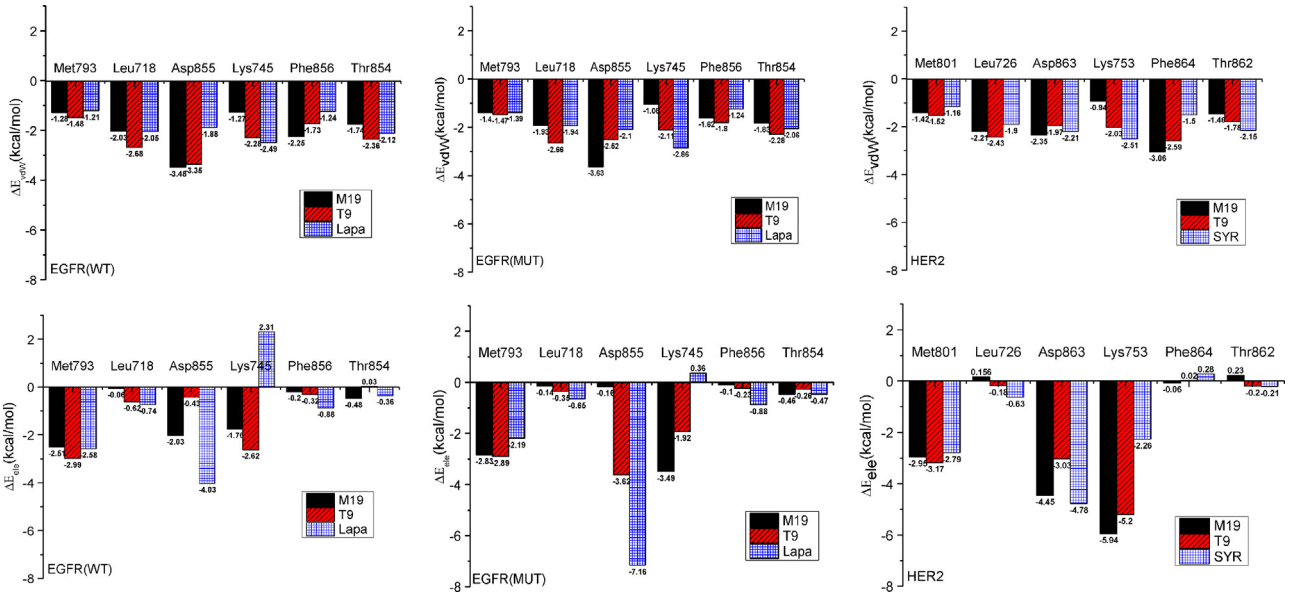


**Fig. 6.** Per-residue binding energy decomposition of the 9 MD runs using the MM-PBSA module of AMBER. M19 complexes are black colored, T9 complexes are red colored and lapatinib complexes are blue colored. Left panel is for EGFR(WT) complexes, middle panel is for EGFR(MUT) complexes and right panel is for HER2 complexes. (For interpretation of references to color in this figure legend, the reader is referred to the web version of this article.)

−3.63 kcal mol$^{-1}$, respectively) than lapatinib (−2.1 kcal mol$^{-1}$). In addition, the Asp855 contribution to the $\Delta E_{ele}$ term in lapatinib binding is given by −7.16 kcal mol$^{-1}$, without direct specific H-bond interactions between Lapatinib and Asp855.

Among the HER2 complexes, M19 receives the largest contribution to the $\Delta E_{vdW}$ from the Phe864 residue (−3.06 kcal mol$^{-1}$). This residue is unique because neither SYR nor lapatinib show a significant contribution to the overall $\Delta E_{vdW}$ term from this residue. The large contribution from this residue to the $\Delta E_{vdW}$ term which results from the additional ring in T9 and M19, indicates that future development of this series of inhibitors should include this residue as an important target. For the $\Delta E_{vdW}$ term, M19 exhibits a larger contribution from the Asp863 residue (−2.35 kcal mol$^{-1}$) than T9 (−1.97 kcal mol$^{-1}$); however, T9 exhibits a larger contribution from Lys753 (−2.03 kcal mol$^{-1}$) compared with M19 (−0.94 kcal mol$^{-1}$) for the same term. For the $\Delta E_{ele}$ term, M19 exhibits larger contributions from both Asp863 (−4.45 kcal mol$^{-1}$) and Lys753 (−5.94 kcal mol$^{-1}$) compared with T9 (−3.03 kcal mol$^{-1}$ and −5.2 kcal mol$^{-1}$, respectively).

## 6. Conclusions

In this study, the binding modes and the mechanisms of inhibition of certain members from a recently synthesized and other *in silico* designed 4-anilinoquinazoline derivatives with a potential inhibitory effect against EGFR and HER2 are studied using long MD simulations and binding energy calculations. It is shown that a substitution at ring "**C**" is important to achieve optimum stability and interaction with the conserved water molecule that is observed frequently in the kinase crystal structures. The new series of inhibitors can bind additional residues in the binding site and utilize direct H-bonding interactions with two amino acid residues, namely, Asp855 and Lys745 for EGFR and Asp863 and Lys753 for HER2. Inclusion of the binding site water molecule in the calculation of the total binding energy results in an energy enhancement of approximately 3–5 kcal mol$^{-1}$, which is caused by an enhancement of the $\Delta E_{ele}$ term. Both MM- and QM/MM-based rescoring methods perform well when predicting the overall trends in the binding energies of the inhibitors.

## Acknowledgments

MA acknowledges the Swinburne University Postgraduate Research Award (SUPRA). FW thanks the Victorian Partnership for Advanced Computing (VPAC) and Swinburne University supercomputing (Green/gSTAR) for the support on the computing facilities. The National Computational Infrastructure (NCI) at the Australian National University and the Victorian Life Sciences Computation Initiative (VLSCI) on its Peak Computing Facility at the University of Melbourne (an initiative of the Victorian Government, Australia) under the National Computational Merit Allocation Scheme (NCMAS) are acknowledged.

## References

[1] J.B. Johnston, S. Navaratnam, M.W. Pitz, J.M. Maniate, E. Wiechec, H. Baust, J. Gingerich, G.P. Skliris, L.C. Murphy, M. Los, Targeting the EGFR pathway for cancer therapy, Current Medicinal Chemistry 13 (2006) 3483–3492.
[2] A. Levitzki, Tyrosine kinase inhibitors: views of selectivity, sensitivity, and clinical performance, Annual Review of Pharmacology and Toxicology 53 (2012) 161–185.
[3] Y. Cheng, W. Cui, Q. Chen, C. -H. Tung, M. Ji, F. Zhang, The molecular mechanism studies of chirality effect of PHA-739358 on Aurora kinase A by molecular dynamics simulation and free energy calculations, Journal of Computer-Aided Molecular Design 25 (2011) 171–180.
[4] K.-W. Wu, P.-C. Chen, J. Wang, Y.-C. Sun, Computation of relative binding free energy for an inhibitor and its analogs binding with Erk kinase using thermodynamic integration MD simulation, Journal of Computer-Aided Molecular Design 26 (2012) 1159–1169.
[5] Z.A. Knight, K.M. Shokat, Features of selective kinase inhibitors, Chemistry & Biology 12 (2005) 621–637.
[6] P. Cohen, Protein kinases: the major drug targets of the twenty-first century? Nature Reviews: Drug Discovery 1 (2002) 309–315.
[7] D. Roymans, H. Slegers, Phosphatidylinositol 3-kinases in tumor progression, European Journal of Biochemistry 268 (2001) 487–498.
[8] M. Malumbres, M. Barbacid, Cell cycle kinases in cancer, Current Opinion in Genetics & Development 17 (2007) 60–65.
[9] H. Daub, K. Specht, A. Ullrich, Strategies to overcome resistance to targeted protein kinase inhibitors, Nature Reviews: Drug Discovery 3 (2004) 1001–1010.
[10] M. Ahmed, M.M. Sadek, R.A. Serrya, A.-H.N. Kafafy, K.A. Abouzid, F. Wang, Assessment of new anti-HER2 ligands using combined docking, QM/MM scoring and MD simulation, Journal of Molecular Graphics and Modelling 40 (2013) 91–98.
[11] M.M. Sadek, R.A. Serrya, A.-H.N. Kafafy, M. Ahmed, F. Wang, K.A.M. Abouzid, Discovery of new HER2/EGFR dual kinase inhibitors based on the anilinoquinazoline scaffold as potential anti-cancer agents, Journal of Enzyme Inhibition and Medicinal Chemistry 1 (2013) 1–8.

[12] T.E. Balius, R.C. Rizzo, Quantitative prediction of fold resistance for inhibitors of EGFR, Biochemistry 48 (2009) 8435–8448.
[13] Y. Yang, J. Qin, H. Liu, X. Yao, Molecular dynamics simulation, free energy calculation and structure-based 3D-QSAR studies of B-RAF kinase inhibitors, Journal of Chemical Information and Modeling 51 (2011) 680–692.
[14] Y. Liu, N.S. Gray, Rational design of inhibitors that bind to inactive kinase conformations, Nature Chemical Biology 2 (2006) 358–364.
[15] A.E. Cho, V. Guallar, B.J. Berne, R. Friesner, Importance of accurate charges in molecular docking: quantum mechanical/molecular mechanical (QM/MM) approach, Journal of Computational Chemistry 26 (2005) 915–931.
[16] J.Y. Chung, J.-M. Hah, A.E. Cho, Correlation between performance of QM/MM docking and simple classification of binding sites, Journal of Chemical Information and Modeling 49 (2009) 2382–2387.
[17] B. Waszkowycz, D.E. Clark, E. Gancia, Outstanding challenges in protein–ligand docking and structure-based virtual screening, WIREs Computational Molecular Science 1 (2011) 229–259.
[18] C.N. Cavasotto, R.A. Abagyan, Protein flexibility in ligand docking and virtual screening to protein kinases, Journal of Molecular Biology 337 (2004) 209–226.
[19] B. Chandrika, J. Subramanian, S.D. Sharma, Managing protein flexibility in docking and its applications, Drug Discovery Today 14 (2009) 394–400.
[20] H.A. Carlson, Protein flexibility is an important component of structure-based drug discovery, Current Pharmaceutical Design 8 (2002) 1571–1578.
[21] E.R. Wood, A.T. Truesdale, O.B. McDonald, D. Yuan, A. Hassell, S.H. Dickerson, B. Ellis, C. Pennisi, E. Horne, K. Lackey, K.J. Alligood, D.W. Rusnak, T.M. Gilmer, L. Shewchuk, A unique structure for epidermal growth factor receptor bound to GW572016 (Lapatinib): relationships among protein conformation, inhibitor off-rate, and receptor activity in tumor cells, Cancer Research 64 (2004) 6652–6659.
[22] K. Aertgeerts, R. Skene, J. Yano, B.C. Sang, H. Zou, G. Snell, A. Jennings, K. Iwamoto, N. Habuka, A. Hirokawa, Structural analysis of the mechanism of inhibition and allosteric activation of the kinase domain of HER2 protein, Journal of Biological Chemistry 286 (2011) 18756–18765.
[23] W. Pao, V.A. Miller, K.A. Politi, G.J. Riely, R. Somwar, M.F. Zakowski, M.G. Kris, H. Varmus, Acquired resistance of lung adenocarcinomas to gefitinib or erlotinib is associated with a second mutation in the EGFR kinase domain, PLoS Medicine 2 (2005) e73.
[24] C.H. Yun, K.E. Mengwasser, A.V. Toms, M.S. Woo, H. Greulich, K.K. Wong, M. Meyerson, M.J. Eck, The T790M mutation in EGFR kinase causes drug resistance by increasing the affinity for ATP, PNAS 105 (2008) 2070–2075.
[25] N. Godin-Heymann, L. Ulkus, B.W. Brannigan, U. McDermott, J. Lamb, S. Maheswaran, J. Settleman, D.A. Haber, The T790M "gatekeeper" mutation in EGFR mediates resistance to low concentrations of an irreversible EGFR inhibitor, Molecular Cancer Therapeutics 7 (2008) 874–879.
[26] T.M. Gilmer, L. Cable, K. Alligood, D. Rusnak, G. Spehar, K.T. Gallagher, E. Woldu, H.L. Carter, A.T. Truesdale, L. Shewchuk, E.R. Wood, Impact of common epidermal growth factor receptor and HER2 variants on receptor activity and inhibition by lapatinib, Cancer Research 68 (2008) 571–579.
[27] Y. Huang, R.C. Rizzo, A water-based mechanism of specificity and resistance for lapatinib with ErbB family kinases, Biochemistry 51 (2012) 2390–2406.
[28] C.-H. Yun, K.E. Mengwasser, A.V. Toms, M.S. Woo, H. Greulich, K.-K. Wong, M. Meyerson, M.J. Eck, The T790M mutation in EGFR kinase causes drug resistance by increasing the affinity for ATP, PNAS 105 (2008) 2070–2075.
[29] J. Stamos, M.X. Sliwkowski, C. Eigenbrot, Structure of the epidermal growth factor receptor kinase domain alone and in complex with a 4-anilinoquinazoline inhibitor, Journal of Biological Chemistry 277 (2002) 46265–46272.
[30] R.A. Friesner, R.B. Murphy, M.P. Repasky, L.L. Frye, J.R. Greenwood, T.A. Halgren, P.C. Sanschagrin, D.T. Mainz, Extra precision glide:docking and scoring incorporating a model of hydrophobic enclosure for protein–ligand complexes, Journal of Medicinal Chemistry 49 (2006) 6177–6196.
[31] Glide, version 5. 7, Schrödinger, LLC, New York, NY, 2011.
[32] V. Aparna, G. Rambabu, S.K. Panigrahi, J.A.R.P. Sarma, G.R. Desiraju, Virtual screening of 4-anilinoquinazoline analogues as EGFR kinase inhibitors: importance of hydrogen bonds in the evaluation of poses and scoring functions, Journal of Chemical Information and Modeling 45 (2005) 725–738.
[33] B. Zhang, V.B.C. Tan, K.M. Lim, T.E. Tay, Significance of water molecules in the inhibition of cylin-dependent kinase 2 and 5 complexes, Journal of Chemical Information and Modeling 47 (2007) 1877–1885.
[34] E. Muzzioli, A. Del Rio, G. Rastelli, Assessing protein kinase selectivity with molecular dynamics and MM-PBSA binding free energy calculations, Chemical Biology & Drug Design 78 (2011) 252–259.
[35] C. Barillari, A.L. Duncan, I.M. Westwood, J. Blagg, R.L.M. van Montfort, Analysis of water patterns in protein kinase binding sites, Proteins: Structure, Function, and Bioinformatics 79 (2011) 2109–2121.
[36] MacroModel, Version 9. 9, Schrödinger, LLC, New York, NY, 2011.
[37] D.A. Case, T.A. Darden, T.E. Cheatham III, C.L. Simmerling, J. Wang, R.E. Duke, R. Luo, R.C. Walker, W. Zhang, K.M. Merz, B. Roberts, S. Hayik, A. Roitberg, G. Seabra, J. Swails, A.W. Goetz, I. Kolossváry, K.F. Wong, F. Paesani, J. Vanicek, R.M. Wolf, J. Liu, X. Wu, S.R. Brozell, T. Steinbrecher, H. Gohlke, Q. Cai, X. Ye, J. Wang, M.-J. Hsieh, G. Cui, D.R. Roe, D.H. Mathews, M.G. Seetin, R. Salomon-Ferrer, C. Sagui, V. Babin, T. Luchko, S. Gusarov, A. Kovalenko, P.A. Kollman, AMBER 12, University of California, San Francisco, 2012.
[38] Y. Duan, C. Wu, S. Chowdhury, M.C. Lee, G. Xiong, W. Zhang, R. Yang, P. Cieplak, R. Luo, T. Lee, J. Caldwell, J. Wang, P. Kollman, A point-charge force field for molecular mechanics simulations of proteins based on condensed-phase quantum mechanical calculations, Journal of Computational Chemistry 24 (2003) 1999–2012.
[39] V. Hornak, R. Abel, A. Okur, B. Strockbine, A. Roitberg, C. Simmerling, Comparison of multiple AMBER force fields and development of improved protein backbone parameters, Proteins: Structure, Function, and Bioinformatics 65 (2006) 712–725.
[40] B. Mennucci, J. Tomasi, R. Cammi, J.R. Cheeseman, M.J. Frisch, F.J. Devlin, S. Gabriel, P.J. Stephens, Polarizable continuum model (PCM) calculations of solvent effects on optical rotations of chiral molecules, Journal of Physical Chemistry A 106 (2002) 6102–6113.
[41] M.J. Frisch, G.W. Trucks, H.B. Schlegel, G.E. Scuseria, M.A. Robb, J.R. Cheeseman, G. Scalmani, V. Barone, B. Mennucci, G.A. Petersson, H. Nakatsuji, M. Caricato, X. Li, H.P. Hratchian, A.F. Izmaylov, J. Bloino, G. Zheng, J.L. Sonnenberg, M. Hada, M. Ehara, K. Toyota, R. Fukuda, J. Hasegawa, M. Ishida, T. Nakajima, Y. Honda, O. Kitao, H. Nakai, T. Vreven, J.A. Montgomery Jr., J.E. Peralta, F. Ogliaro, M. Bearpark, J.J. Heyd, E. Brothers, K.N. Kudin, V.N. Staroverov, R. Kobayashi, J. Normand, K. Raghavachari, A. Rendell, J.C. Burant, S.S. Iyengar, J. Tomasi, M. Cossi, N. Rega, J.M. Millam, M. Klene, J.E. Knox, J.B. Cross, V. Bakken, C. Adamo, J. Jaramillo, R. Gomperts, R.E. Stratmann, O. Yazyev, A.J. Austin, R. Cammi, C. Pomelli, J.W. Ochterski, R.L. Martin, K. Morokuma, V.G. Zakrzewski, G.A. Voth, P. Salvador, J.J. Dannenberg, S. Dapprich, A.D. Daniels, Ö. Farkas, J.B. Foresman, J.V. Ortiz, J. Cioslowski, D.J. Fox, Gaussian 09, Revision A.1, Gaussian, Inc., Wallingford CT, 2009.
[42] C.I. Bayly, P. Cieplak, W. Cornell, P.A. Kollman, A well-behaved electrostatic potential based method using charge restraints for deriving atomic charges: the RESP model, Journal of Physical Chemistry 97 (1993) 10269–10280.
[43] J. Wang, R.M. Wolf, J.W. Caldwell, P.A. Kollman, D.A. Case, Development and testing of a general AMBER force field, Journal of Computational Chemistry 25 (2004) 1157–1174.
[44] W.L. Jorgensen, J. Chandrasekhar, J.D. Madura, R.W. Impey, M.L. Klein, Comparison of simple potential functions for simulating liquid water, Journal of Chemical Physics 79 (1983) 926–935.
[45] J.-P. Ryckaert, G. Ciccotti, H.J.C. Berendsen, Numerical integration of the Cartesian equations of motion of a system with constraints: molecular dynamics of n-alkanes, Journal of Computational Physics 23 (1977) 327–341.
[46] H.J.C. Berendsen, J.P.M. Postma, W.F. van Gunsteren, A. DiNola, J.R. Haak, Molecular dynamics with coupling to an external bath, Journal of Chemical Physics 81 (1984) 3684–3690.
[47] T. Darden, D. York, L. Pedersen, Particle mesh Ewald: an $N\log(N)$ method for Ewald sums in large systems, Journal of Chemical Physics 98 (1993) 10089–10092.
[48] B.R. Miller, T.D. McGee, J.M. Swails, N. Homeyer, H. Gohlke, A.E. Roitberg, MMPBSA.py: an efficient program for end-state free energy calculations, Journal of Chemical Theory and Computation 8 (2012) 3314–3321.
[49] Prime, Version 3. 0, Schrödinger, LLC, New York, 2011.
[50] M.P. Jacobson, D.L. Pincus, C.S. Rapp, T.J.F. Day, B. Honig, D.E. Shaw, R.A. Friesner, A hierarchical approach to all-atom protein loop prediction, Proteins: Structure, Function, and Bioinformatics 55 (2004) 351–367.
[51] J. Du, H. Sun, L. Xi, J. Li, Y. Yang, H. Liu, X. Yao, Molecular modeling study of checkpoint kinase 1 inhibitors by multiple docking strategies and prime/MM–GBSA calculation, Journal of Computational Chemistry 32 (2011) 2800–2809.
[52] R.C. Walker, M.F. Crowley, D.A. Case, The implementation of a fast and accurate QM/MM potential method in AMBER, Journal of Computational Chemistry 29 (2007) 1019–1031.
[53] J.P. McNamara, I.H. Hillier, Semi-empirical molecular orbital methods including dispersion corrections for the accurate prediction of the full range of intermolecular interactions in biomolecules, Physical Chemistry Chemical Physics 9 (2007) 2362–2370.
[54] F. Gräter, S.M. Schwarzl, A. Dejaegere, S. Fischer, J.C. Smith, Protein/ligand binding free energies calculated with quantum mechanics/molecular mechanics, The Journal of Physical Chemistry B 109 (2005) 10474–10483.
[55] R. Villar, M.J. Gil, J.I. García, V. Martínez-Merino, Are AM1 ligand–protein binding enthalpies good enough for use in the rational design of new drugs? Journal of Computational Chemistry 26 (2005) 1347–1358.
[56] C.N. Alves, S. Martí, R. Castillo, J. Andrés, V. Moliner, I. Tuñón, E. Silla, A quantum mechanics/molecular mechanics study of the protein–ligand interaction for inhibitors of HIV-1 integrase, Chemistry: A European Journal 13 (2007) 7715–7724.
[57] P. Traxler, P. Furet, Strategies toward the design of novel and selective protein tyrosine kinase inhibitors, Pharmacology & Therapeutics 82 (1999) 195–206.
[58] M.E.M. Noble, J.A. Endicott, L.N. Johnson, Protein kinase inhibitors: insights into drug design from structure, Science Signaling 303 (2004) 1800–1805.
[59] K. Oruganty, N. Kannan, Design principles underpinning the regulatory diversity of protein kinases, Philosophical Transactions of the Royal Society B: Biological Sciences 367 (2012) 2529–2539.
[60] F. Zuccotto, E. Ardini, E. Casale, M. Angiolini, Through the "Gatekeeper Door": exploiting the active kinase conformation, Journal of Medicinal Chemistry 53 (2009) 2681–2694.
[61] M.E.M. Noble, J.A. Endicott, L.N. Johnson, Protein kinase inhibitors: insights into drug design from structure, Science Signalling 303 (2004) 1800–1805.
[62] N. Songtawee, M.P. Gleeson, K. Choowongkomon, Computational study of EGFR inhibition: molecular dynamics studies on the active and inactive protein conformations, Journal of Molecular Modeling 19 (2012) 1–13.
[63] M.A. Seeliger, P. Ranjitkar, C. Kasap, Y. Shan, D.E. Shaw, N.P. Shah, J. Kuriyan, D.J. Maly, Equally potent inhibition of c-Src and Abl by compounds that recognize inactive kinase conformations, Cancer Research 69 (2009) 2384–2392.

[64] M.A. Bogoyevitch, D.P. Fairlie, A new paradigm for protein kinase inhibition: blocking phosphorylation without directly targeting ATP binding, Drug Discovery Today 12 (2007) 622–633.
[65] S. Yoshikawa, M. Kukimoto-Niino, L. Parker, N. Handa, T. Terada, T. Fujimoto, Y. Terazawa, M. Wakiyama, M. Sato, S. Sano, Structural basis for the altered drug sensitivities of non-small cell lung cancer-associated mutants of human epidermal growth factor receptor, Oncogene 32 (2012) 27–38.
[66] M. Muhsin, J. Graham, P. Kirkpatrick, Gefitinib, Nature Reviews: Drug Discovery 2 (2003) 515–516.
[67] M.H. Nelson, C.R. Dolder, Lapatinib: a novel dual tyrosine kinase inhibitor with activity in solid tumors, The Annals of Pharmacotherapy 40 (2006) 261–269.
[68] F. Montemurro, G. Valabrega, M. Aglietta, Lapatinib: a dual inhibitor of EGFR and HER2 tyrosine kinase activity, Expert Opinion on Biological Therapy 7 (2007) 257–268.
[69] T.E. Balius, R.C. Rizzo, T.E. Balius, R.C. Rizzo, Quantitative prediction of fold resistance for inhibitors of EGFR, Biochemistry 48 (2009) 8435–8448.
[70] S.-Y. Lu, Y.-J. Jiang, J. Lv, J.-W. Zou, T.-X. Wu, Role of bridging water molecules in GSK3β-inhibitor complexes: Insights from QM/MM, MD, and molecular docking studies, Journal of Computational Chemistry 32 (2011) 1907–1918.
[71] M. Kaur, M.S. Bahia, O. Silakari, Exploring the role of water molecules for docking and receptor guided 3D-QSAR analysis of naphthyridine derivatives as spleen tyrosine kinase (Syk) inhibitors, Journal of Chemical Information and Modeling 52 (2012) 2619–2630.
[72] G.W. Rewcastle, W.A. Denny, A.J. Bridges, H. Zhou, D.R. Cody, A. McMichael, D.W. Fry, Tyrosine kinase inhibitors. 5. Synthesis and structure-activity relationships for 4-[(phenylmethyl)amino]- and 4-(phenylamino)quinazolines as potent adenosine 5′-triphosphate binding site inhibitors of the tyrosine kinase domain of the epidermal growth factor receptor, Journal of Medicinal Chemistry 38 (1995) 3482–3487.
[73] A. Wissner, D.M. Berger, D.H. Boschelli, M.B. Floyd Jr., L.M. Greenberger, B.C. Gruber, B.D. Johnson, N. Mamuya, R. Nilakantan, ReichF F.M., 4-Anilino-6,7-dialkoxyquinoline-3-carbonitrile inhibitors of epidermal growth factor receptor kinase and their bioisosteric relationship to the 4-anilino-6, 7-dialkoxyquinazoline inhibitors, Journal of Medicinal Chemistry 43 (2000) 3244–3256.
[74] D.H. Boschelli, 4-Anilino-3-quinolinecarbonitriles: an emerging class of kinase inhibitors, Current Topics in Medicinal Chemistry 2 (2002) 1051–1063.
[75] S. Nandi, M. Bagchi, 3D-QSAR and molecular docking studies of 4-anilinoquinazoline derivatives: a rational approach to anticancer drug design, Molecular Diversity 14 (2010) 27–38.
[76] A.J. Bridges, H. Zhou, D.R. Cody, G.W. Rewcastle, A. McMichael, H.D.H. Showalter, D.W. Fry, A.J. Kraker, W.A. Denny, Tyrosine kinase inhibitors. 8. An unusually steep structure–activity relationship for analogues of 4-(3-bromoanilino)-6,7-dimethoxyquinazoline (PD 153035), a potent inhibitor of the epidermal growth factor receptor, Journal of Medicinal Chemistry 39 (1996) 267–276.
[77] S. Kamath, J.K. Buolamwini, Targeting EGFR and HER2 receptor tyrosine kinases for cancer drug discovery and development, Medicinal Research Reviews 26 (2006) 569–594.
[78] V.G. Pawar, M.L. Sos, H.B. Rode, M. Rabiller, S. Heynck, W.A.L. van Otterlo, R.K. Thomas, D. Rauh, Synthesis and biological evaluation of 4-anilinoquinolines as potent inhibitors of epidermal growth factor receptor, Journal of Medicinal Chemistry 53 (2010) 2892–2901.
[79] B. Liu, B. Bernard, J.H. Wu, Impact of EGFR point mutations on the sensitivity to gefitinib: insights from comparative structural analyses and molecular dynamics simulations, Proteins: Structure, Function, and Bioinformatics 65 (2006) 331–346.
[80] A.F. Gazdar, Activating and resistance mutations of EGFR in non-small-cell lung cancer: role in clinical response to EGFR tyrosine kinase inhibitors, Oncogene 28 (2009) S24–S31.
[81] K.-S.H. Nguyen, S. Kobayashi, D.B. Costa, Acquired resistance to epidermal growth factor receptor tyrosine kinase inhibitors in non-small-cell lung cancers dependent on the epidermal growth factor receptor pathway, Clinical Lung Cancer 10 (2009) 281–289.
[82] R. Dienstmann, S. De Dosso, E. Felip, J. Tabernero, Drug development to overcome resistance to EGFR inhibitors in lung and colorectal cancer, Molecular Oncology 6 (2012) 15–26.
[83] W. Zhou, D. Ercan, L. Chen, C.H. Yun, D. Li, M. Capelletti, A.B. Cortot, L. Chirieac, R.E. Iacob, R. Padera, Novel mutant-selective EGFR kinase inhibitors against EGFR T790M, Nature 462 (2009) 1070–1074.
[84] T. Hou, J. Wang, Y. Li, W. Wang, Assessing the performance of the molecular mechanics/Poisson Boltzmann surface area and molecular mechanics/generalized Born surface area methods. II. The accuracy of ranking poses generated from docking, Journal of Computational Chemistry 32 (2011) 866–877.
[85] T. Hou, J. Wang, Y. Li, W. Wang, Assessing the performance of the MM/PBSA and MM/GBSA Methods. 1. The accuracy of binding free energy calculations based on molecular dynamics simulations, Journal of Chemical Information and Modeling 51 (2010) 69–82.